Inversion of roughness parameters of self-affine surfaces from backscattered waves

Stéphanie Gautier, Dominique Gibert

Geophys. J. Int. (2005) **160,** 797–803 doi: 10.1111/j.1365-246X.2005.02500.x

Inversion of roughness parameters of self-affine surfaces from backscattered waves

Stéphanie Gautier[1]* and Dominique Gibert[2]

[1] *Géosciences Azur (CNRS/INSU UMR* 6526*),* 250 *Avenue Albert Einstein,* 06560 *Valbonne, France. E-mail: stephanie.gautier@geoazur.unice.fr*
[2] *Géosciences Rennes (CNRS/INSU UMR* 6118*), Bât.* 15, *Campus de Beaulieu,* 35042 *Rennes Cedex, France. E-mail: dominique.gibert@univ-rennes1.fr*

Accepted 2004 October 11. Received 2004 October 7; in original form 2004 March 1

SUMMARY

We propose an inverse method to recover the roughness parameters (altitude range Δh_0, and Hurst exponent H) of self-affine surfaces from the energy spectrum of backscattered waves. A stochastic forward modelling of the spectrum of the backscattered wavefield averaged along a profile of finite length is proposed in the near-nadir and far-field configuration. A Bayesian formulation of the inverse problem is used to account for the random nature of both the data and the forward problem. An acoustic backscattering experiment is performed with a natural rough self-affine surface for which Δh_0 and H are determined through direct measurements of the topography. The inversion of the experimental spectrum of the backscattered acoustic waves shows that a good determination of H is possible, while Δh_0 is an unresolved parameter.

Key words: Bayesian inversion, fractal, Hurst exponent, surface characterization, wave scattering.

1 INTRODUCTION

The determination of the roughness of natural interfaces is an important issue in many areas of Earth sciences. Roughness properties such as amplitude, correlation length, Fourier spectra, coda waves, etc. are known to give important information on the origin of these interfaces and on the alteration processes acting on them. Many rough interfaces have been shown to possess self-affine, or fractal, roughness properties, i.e. a roughness appearance independent of the scale of observation and having a long-range correlation (Mandelbrot 1975; Turcotte 1989; Gouyet 1992). The roughness of fractal interfaces is controlled by the fractal dimension D or, equivalently, by the Hurst exponent $H = d - D$, where d is the dimension of the space embedding the interface. The Hurst exponent, H, controls the roughness amplitude $\langle \Delta h_L \rangle$ statistically observed at a given scale L by means of the statistical homogeneity relationship

$$\langle \Delta h_L \rangle = \langle \Delta h_0 \rangle \left(\frac{L}{L_0} \right)^H, \tag{1}$$

where $\langle \Delta h_0 \rangle$ is the average amplitude range for the observation scale L_0 taken as a reference length. In this paper, L_0 is arbitrarily taken as the maximum size of the observation profile or area of the rough surface. In practice, $\langle \Delta h_L \rangle$ may be any geometrical quantity uniquely defined at a given observation scale L such as, for instance, the average range spanned by the vertical axis when plotting a region of width L in the rough surface (Feder 1988). Fig. 1(a) shows three synthetic self-affine profiles corresponding to different values of H. These profiles have been generated using the Fourier method (Fox 1987) and with the same random phase spectrum in order to give them a common appearance. It can be seen that profiles with larger H values look like low-pass-filtered versions of profiles with smaller H.

The determination of either the fractal dimension, D, or the Hurst exponent, H, of topography data constitutes a way to perform landform classification and may give insight into the evolution processes, build-up and/or erosion, at work (Burrough 1981; Milne 1988). Similar results are obtained from the analysis of seafloor roughness (Fox & Hayes 1985; Smith & Shaw 1989). Fractures also display a fractal roughness (Okubo & Aki 1987), and geochemical processes occurring during fluid circulation in fractures strongly depend on the edge roughness, which controls both the hydraulic conductivity and the exchange area between the fluid and the rock matrix (Brown 1989; Thompson & Brown 1991; Meheust & Schmittbuhl 2000).

A straightforward approach to describing and analysing the roughness of a surface is to measure its topography directly and analyse the data thus obtained (Schmittbuhl *et al.* 1993). However, many surfaces, among which those cited above, are either too large or too remote to allow such a direct analysis. Consequently their roughness properties must be determined indirectly by using remote sensing methods such as radars to describe terrestrial soil roughness (Zribi *et al.* 2000) and geomorphological characterization of the surface of other planets (Shepard *et al.* 2001; Campbell & Shepard 1996). Acoustic waves may also be used to probe the seafloor (Mourad & Jackson 1993; Lyons *et al.* 1994; Jackson *et al.* 1996; Lurton 2002). In these cases, the roughness parameters must be extracted from information carried by the waves backscattered by the surface of interest (Goff & Jordan 1989).

*Formerly with Géosciences Rennes.

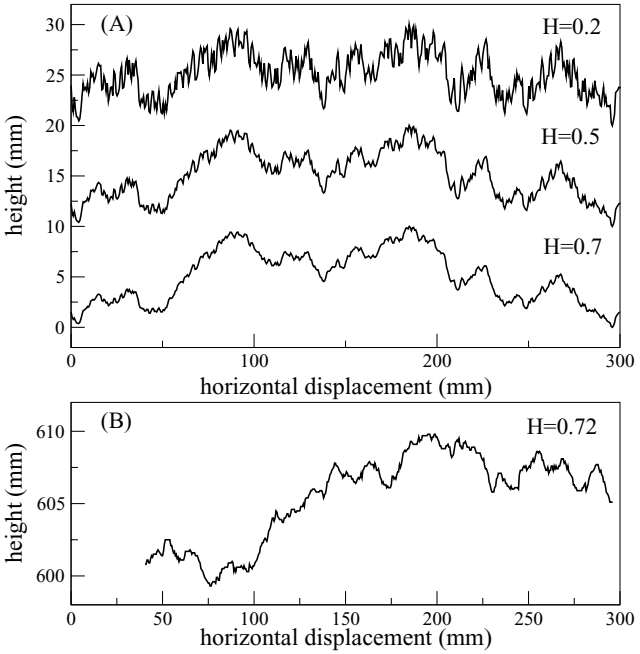

Figure 1. (a) Three synthetic self-affine profiles showing the roughness dependence with respect to the Hurst exponent H. These profiles have a similar appearance because they have been generated by the Fourier transform method with the same random phase spectrum and $\Delta h_0 = 10.5$ mm. The main influence of the Hurst exponent is to change the amplitude of the short wavelengths relative to that of the long wavelengths. (b) Example of a profile (in the y direction) extracted from the experimental rough surface used in this study. The roughness appearance of this profile is more similar to that of the synthetic profile with $H = 0.70$.

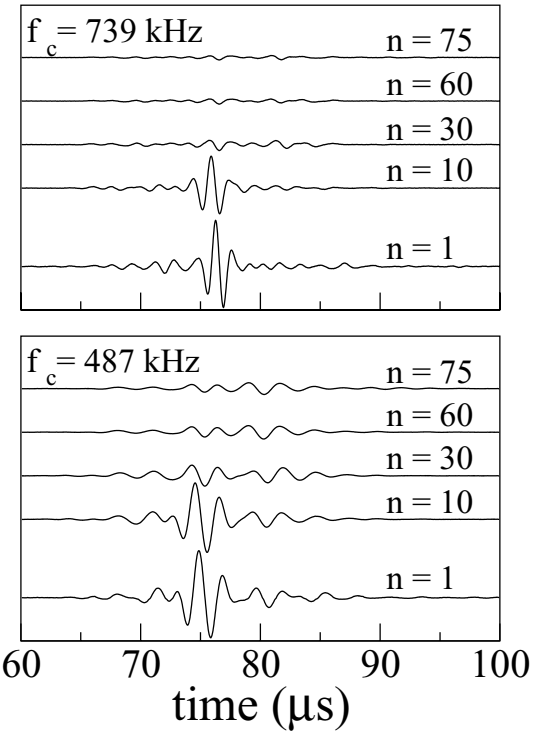

Figure 2. Average records of acoustic waves reflected by a self-affine rough surface and corresponding to a source signal with central frequencies $f_c = 487$ kHz (bottom) and $f_c = 739$ kHz (top). The averaged signals have been computed for various numbers n of individual signals recorded along a straight profile. The larger the value of n, the smaller the amplitude of the average signal.

Wave scattering from rough surfaces has been extensively studied for a long time (Beckmann & Spizzichino 1963), and there is considerable literature on the subject (see e.g. Ogilvy 1991; Voronovich 1994; Ishimaru 1997 for detailed reviews). Most of these studies, however, consider surfaces with a moderate roughness often assumed to be stationary and random Gaussian. These nice statistical properties are generally introduced for mathematical convenience but they are not satisfied by rough interfaces with a fractal-like roughness (Sayles & Thomas 1978).

Since the pioneering study of Berry (1979) (see also Berry & Blackwell 1981) numerous papers have dealt with the particular problem of wave scattering by fractal interfaces, with applications to many scientific domains such as oceanography (Chen *et al.* 1994) and optics (Jaggar & Sun 1990). However, wave scattering by fractal surfaces remains challenging because of the long-range correlation of the relief observed along profiles (Simonsen *et al.* 2000). Indeed, as eq. (1) indicates, the longer the walk along the surface the larger the height variations observed (Fig. 1). In practice, this means that, as one moves along a profile above the surface with a source and an antenna recording the waves reflected by the rough topography, the backscattered waves arrive at the receiver with random phase lags whose maximum amplitude increases as the length of the path increases. Consequently, classically used quantities such as the mean backscattered wavefield cannot be given the same sense as for random stationary rough surfaces because, as the size of the averaging profile (or surface) increases, the average of the backscattered signals rapidly converges to zero. This occurs because as the length of the path along the profile increases, the individual signals stacked to form the average signals are more and more (in a statistical sense) out of phase. The stack is then gradually annihilated to give an asymptotically vanishing sum (Papoulis 1984).

Fig. 2 shows the average wavefields reflected by the self-affine surface used in the remainder of this study and corresponding to a source signal given by eq. (2) for central frequencies $f_c = 487$ kHz and $f_c = 739$ kHz. The average signals have been computed using a number n of individual adjacent signals recorded along a straight profile above the surface. It can be seen that the amplitude of the average signal dramatically decreases as n increases, and, because of the self-affine nature of the rough surface, this phenomenon occurs at all frequencies (i.e. wavelengths λ). In contrast, in the case of stationary rough surfaces, there exists a corner wavelength beyond which such a decrease is not observed because the phase lags are too small to produce significant destructive interferences in the stacking procedure. The self-affine property of the rough surface implies that the rms amplitude of the average signals decreases by an amount proportional to n/λ, a rule roughly satisfied by the signals shown in Fig. 2. This behaviour is a direct consequence of the long-range correlation of self-affine surfaces and leads to two major difficulties for the probing of fractal rough surfaces with backscattered waves: (1) there is no critical averaging size (either surface area or profile length) beyond which the averaged backscattered waves can be considered arbitrarily close to a non-null asymptotic mean field corresponding to an infinite averaging size; (2) the averaged quantities obtained display strong variations from one averaging profile to another. This last point indicates that a large part of the wave scattering produced by a fractal topography must be considered to occur in the mesoscopic-scale range, where the classical statistics of large numbers is useless. Instead, it is necessary to explicitly

account for the fact that the data obtained for a single averaging profile are a single drawing from a set of strongly fluctuating realizations. These difficulties make the characterization of fractal surfaces from backscattered waves very different from the approach used for non-fractal and stationary rough surfaces (Berry 1972).

In the present study we show how the strong fluctuations occurring at mesoscopic scales may be accounted for in an inversion procedure to recover the roughness characteristics of a self-affine rough surface from backscattered waves averaged along a single profile with a finite length. In order to make the paper self-consistent, we first present the main aspects of the data obtained through an acoustic experiment performed in a water tank with a fractal rough surface. Next, we discuss the numerical modelling (i.e. the direct problem) of the measured backscattered waves. In the last section, a Bayesian inversion is performed by considering the direct problem as a fuzzy stochastic physical model.

2 EXPERIMENTAL WAVELET RESPONSE OF ROUGH SURFACES

In this section we present the experimental data which are inverted in the last section of this paper. The rough surface used in the present study is a synthetic resin print of a natural surface obtained by fracturing a granite block. By using a homogeneous resin print instead of the natural surface itself we limit the diffraction effects to those created by the rough surface and eliminate the diffracted waves that could be produced by the mineral grains inside the granite block. The topography of the resin surface has been digitized with a laser profiler, and a profile extracted from the digitized topography is shown in Fig. 1(b). An analysis of the digitized topography confirms its self-affine nature with a Hurst exponent of $H \simeq 0.72$, typical of long-range correlated height variations (Gautier & Gibert 2004).
The backscattering experiment is performed in a large water-tank (5 m^3) with the experimental setup shown in Fig. 3. An arbitrary waveform generator triggers a power amplifier which fires a piezoelectric source located above the rough surface and directed in a near-nadir direction. The waves backscattered by the rough topography are recorded with another piezo-electric transducer placed near the source. This second transducer is necessary because the source transducer controlled by the arbitrary waveform generator cannot be switched sufficiently rapidly to be used as a receiver. The rough surface can be rolled-along in order to record the backscattered wavefield along a straight profile.

The numerical signals sent to the source by the arbitrary waveform generator are obtained through a non-linear inversion algorithm (Conil *et al.* 2004) in such a way that the waves reflected by a flat reference surface are pure self-similar wavelets $\Psi_a(t)$ defined by

$$\Psi_a(t) = \frac{1}{a}\frac{d^4}{d(t/a)^4}\exp\left(-\frac{t^2}{a^2}\right). \qquad (2)$$

The dilation $a > 0$ controls the duration of the wavelets whose energy spectrum is bandpass-like with a central frequency $f_c \propto a^{-1}$. The temporal localization of the wavelet allows the waves reflected by the surface to be separated from those coming from other parts of the apparatus such as the flat bottom face of the resin print. Seven pairs of transducers with central frequencies varying from 250 kHz to 2.5 MHz are used, and the frequency range covered by the wavelet family goes from 172 kHz to 2.572 MHz, corresponding to wavelengths ranging from 8.7 to 0.6 mm in water. All transducers have identical active surface areas with a diameter $D = 25$ mm. The focal distance $d_f = D^2/4\lambda$ (Angelsen 2000) which separates the near-field

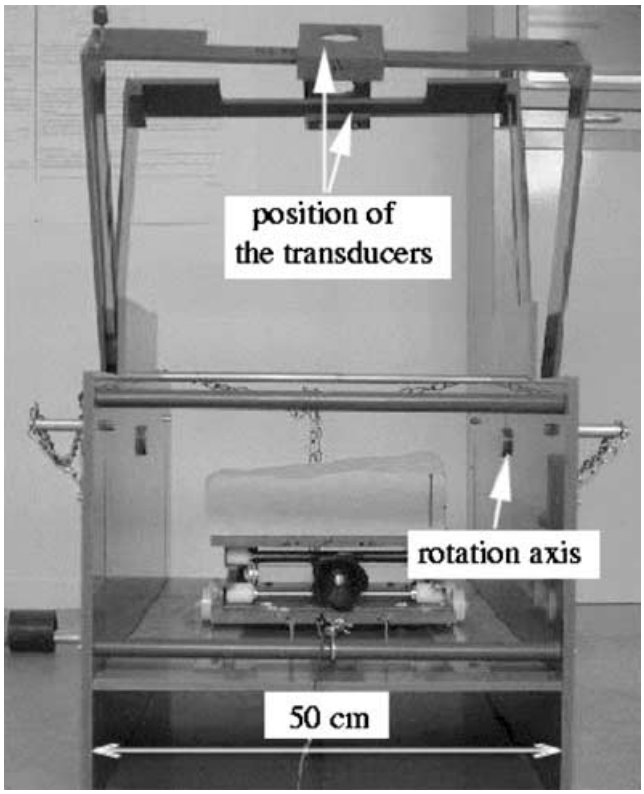

Figure 3. View of the experimental setup used in this study. The rough surface is placed on a moving plate which can be rolled under the piezoelectric transducers (source and receiver) located above.

Fresnel zone from the far-field Fraunhofer zone varies from 18 mm at the lowest frequencies to 260 mm at the highest frequencies. The distance $l_e = 600$ mm between the transducers and the rough surface was kept constant to satisfy the far-field conditions at all frequencies. Each pair of transducers is used to span a wavelength range to construct the entire wavelet family, i.e. several wavelets with nearby wavelengths are produced with the same transducers.

The use of optimized source signals gives reflected signals with a high signal-to-noise ratio and enables an accurate study of the frequency-dependent response of the target. A great advantage of this experimental procedure is that no post-deconvolution of the output signals is necessary, and the reflected waves for each optimized source signal can be directly recorded to constitute what will hereafter be called *the wavelet response* of the target surface.

For each wavelet source, a total of 75 wavelet responses like those shown in Fig. 2 for $n = 1$ were recorded along a 18.5-cm long profile with a constant sampling interval. These individual wavelet responses were stacked to obtain the average wavelet response, as shown in Fig. 2 for $n = 75$. The total energy of the average wavelet responses is computed to obtain the energy spectrum of the backscattered waves, and this constitutes the data used in the inversion presented below (Fig. 5).

3 STOCHASTIC MODELLING

The mean backscattered field, $\langle \psi_f \rangle$, is computed with a modified version of the model proposed by Shepard & Campbell (1999) (Gautier & Gibert 2004). The model is based on the Helmholtz–Kirchhoff diffraction formula (Elmore & Heald 1985; Ishimaru 1997), and the backscattered field is computed by representing the rough

topography as an ensemble of point scatterers excited by a plane wave with normal incidence and amplitude ψ_0. Multiple scattering among the point scatterers is neglected, and the individual contributions of the scatterers can then be summed in any order to obtain the total field $\langle\psi_f\rangle$. A far-field and near-nadir geometry is assumed so that the obliquity factor can be omitted. In a cylindrical coordinate system (r, φ) with the $r = 0$ axis oriented in the incident normal direction and passing through the observation point P, the backscattered wavefield ψ_f can be approximated as (Gautier & Gibert 2004)

$$\psi_f(P) \simeq -\frac{i\psi_0}{\lambda}\frac{e^{ikl_e}}{l_e}\int_0^R r\,dr\int_0^{2\pi} e^{-2ikh(r,\varphi)}\,d\varphi, \tag{3}$$

where $k = 2\pi f/c$ is the wavenumber, f is the frequency, c is the wave velocity, and l_e is the distance between the observation point P and its normal projection P_s on the surface. The surface topography $h(r, \varphi)$ is measured with respect to the altitude of P_s [i.e. $h(P_s) = 0$].

The mean field $\langle\psi_f\rangle$ is obtained by averaging the backscattered field measured along a y profile of length L:

$$\langle\psi_f\rangle_L = -\frac{i\psi_0}{L\lambda}\int_0^L \frac{e^{ikl_e(y)}}{l_e(y)}dy\int_0^R r\,dr\int_0^{2\pi} e^{-2ikh(r,\varphi)}\,d\varphi, \tag{4}$$

and the energy spectrum is given by

$$E(f) = |\langle\psi_f\rangle_L|^2 = \left|\langle\psi_f\rangle_L\langle\psi_f\rangle_L^*\right|, \tag{5}$$

where * indicates the complex conjugate of the mean field.

The mean backscattered wavefield given by eq. (4) is computed through three integrals. The rightmost one is over a circle of radius r, and the middle one sums the contributions of all circles for $0 \le r \le R$ to give the total field backscattered by a circular disc of radius R (see also eq. 3). The leftmost integral sums the contributions of all discs along a path of length L. If $L \gg R$, the mean backscattered field results from a large number of discs, and it is possible to replace the integration over φ by a stochastic integral using the statistical distribution of $h(r, \varphi)$. Because of the self-affine nature of the rough surface, the topography $h(r, \varphi)$ measured along circles of radius r has Gaussian statistics with a standard deviation $\sigma_c(r) = \sigma_c(r_0)(r/r_0)^H$, where r_0 is an arbitrary reference radius (Gautier & Gibert 2004). This means that an analytical evaluation of the rightmost integral in eq. (4) can be performed by replacing the φ integral by one over the h distribution at a given r. We obtain

$$\langle\psi_f\rangle_L = -\frac{i\psi_0}{L\lambda}\int_0^L \frac{e^{ikl_e(y)}}{l_e(y)}dy\int_0^R e^{-2k^2\sigma_c^2(r)}r\,dr, \tag{6}$$

where the rightmost integral can easily be evaluated numerically using standard algorithms (Press *et al.* 1992).

The y integral cannot be evaluated in the same way because it involves a single profile of finite length L and no ensemble averaging can be inferred to enable use of the probability distribution of $l_e(y)$. Indeed, this integration is the one that accounts for the mesoscopic scales that produce the strong fluctuations in the mean-field realizations from one profile to another. It is, then, important to preserve these phenomena when computing the y integral. This is done by a numerical integration along a random synthetic $l_e(y)$ profile of length L with both a given Hurst exponent H and an amplitude range Δh_0. By using this procedure, we preserve the long-range correlation observed in real data (Fig. 1b). The forward problem given by eq. (6) can be seen as a stochastic process since its output randomly changes for each particular realization of the $l_e(y)$ profile used in the numerical integration.

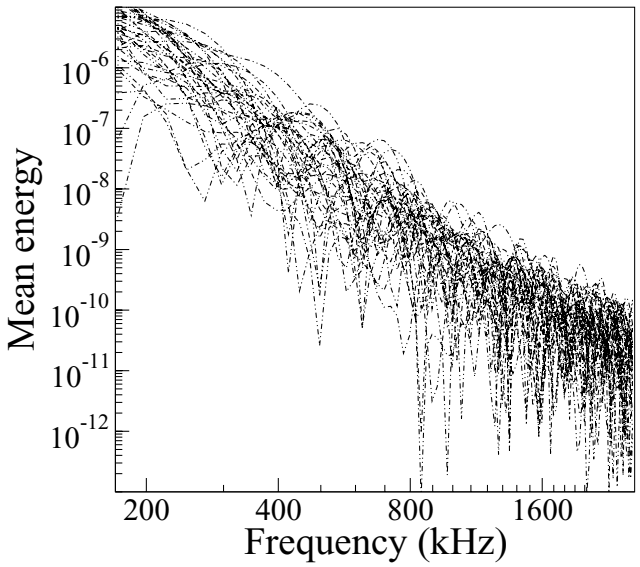

Figure 4. Synthetic energy spectra obtained from a set of runs of the stochastic forward problem. The distribution of the synthetic spectra is used to derive the probability distribution ρ_s to be used in the Bayesian inference formula as shown in Fig. 5.

A different energy spectrum is obtained for each realization of a $l_e(y)$ profile in eq. (6), as shown in Fig. 4, and the set of spectra thus obtained is used to compute an estimate of the probability density function, $\rho_s(f, E)$, representing the statistical distribution of the energy spectra produced by rough surfaces with a given Hurst exponent. In practice, the probability ρ_s is computed from a set of 100 individual spectra (Fig. 5), and the probability density function $\rho_s(f, E)$ is the output of the stochastic direct problem, which constitutes the relevant quantity to be compared with the experimental spectra obtained during the acoustic experiments (Tarantola & Valette 1982).

4 BAYESIAN INVERSION

We now present a Bayesian inversion based on the stochastic forward modelling presented in the previous section and given by eq. (6). The parameters to be fixed in order to compute a single realization of the stochastic process (6) are the length L of the averaging profile, the wavelength λ, the integration radius R, the amplitude ψ_0 of the incident plane wave, the standard deviation $\sigma_c(r_0)$, the amplitude range Δh_0 of the $l_e(y)$ profiles, and the Hurst exponent H. Each of these parameters may either be kept fixed during the inversion or be considered as an unknown parameter to be determined through the inversion.

Both L and λ are known from the experimental characteristics of the data to be inverted and they can be given a value at the beginning of the inversion process. The radius R is the size of the circular spot (with centre P_s) onto the rough surface where the point scatterers coherently reradiate to produce the measured backscattered wavefield. R is defined as the limit beyond which the rightmost integral in eq. (6) reaches a plateau, and it is automatically determined in the numerical integration procedure by checking the convergence of the integral for parameters (source/receiver distance and geometry) corresponding to the experimental conditions (Gautier & Gibert 2004).

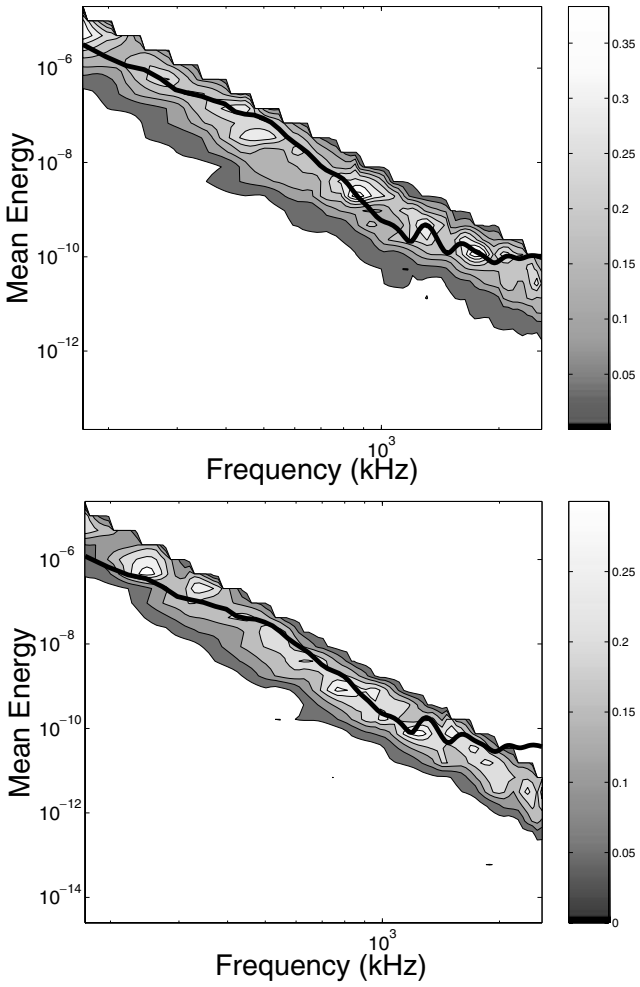

Figure 5. Solid line: energy spectrum of the experimental backscattered wavefield averaged along a profile of length $L = 185$ mm. Grey contour maps: probability distribution ρ_s of the synthetic spectra produced by the stochastic forward problem. Top: distribution obtained for the best inverted model with $\Delta h_0 = 12$ mm, $H = 0.74$ (black star in Fig. 6). Bottom: distribution corresponding to $\Delta h_0 = 14$ mm, $H = 0.66$ (white circle in Fig. 6).

The amplitude ψ_0 is a linear parameter that fixes the absolute level of the synthetic spectra. This amplitude should ideally be known from the characteristics of the experiment but, in practice, an accurate knowledge of ψ_0 is possible only for very well controlled experimental conditions, as in the experiments discussed in this study. This is obviously not the case for most geophysical experiments, where the aim is to invert the data with the method proposed in this paper. Consequently, in this study, the parameter ψ_0 is supposed unknown and is determined during the inversion. However, this parameter is treated as an adjustable parameter whose value is chosen in order to maximize the posterior probability ρ_p at each $(\Delta h_0, H)$ point in the parameter space (see for instance Gibert & Virieux 1991 for such an approach).

The remaining three parameters, $\sigma_c(r_0)$, Δh_0 and H, directly depend on the roughness properties of the scattering surface and are the parameters to be determined. However, the standard deviation $\sigma_c(r_0)$ is a secondary parameter whose value is totally determined by both Δh_0 and H, which are the two independent primary parameters considered here. We emphasize that Δh_0 could be taken as the secondary parameter instead of $\sigma_c(r_0)$. During sensitivity tests, we observed that the spectral slope is weakly affected when either Δh_0 or $\sigma_c(r_0)$ vary in reasonable bounds. This indicates that Δh_0 will probably be a poorly resolved parameter. On the other hand, the same sensitivity tests showed that small changes of H produce significant variations of the spectral slope.

According to the discussion just above, the statistical distribution of the synthetic spectra is written as $\rho_s(\Delta h_0, H)$, where only the inverted parameters appear explicitly. The solution of the inverse problem is the posterior probability density $\rho_p(\Delta h_0, H|\text{data})$, which can be obtained using Bayes' rule:

$$\rho_p(\Delta h_0, H|\text{data}) = \frac{\rho(\Delta h_0, H)\rho(\text{data}|\Delta h_0, H)}{\int\int \rho(\Delta h_0, H)\rho(\text{data}|\Delta h_0, H)d\Delta h_0 dH}, \quad (7)$$

where $\rho(\Delta h_0, H)$ is the prior probability of the parameters, and $\rho(\text{data}|\Delta h_0, H)$ is the conditional probability of the data for given values of the parameters. The integral in the denominator of (7) is over the parameter space and is a normalizing factor which can be omitted.

The conditional probability $\rho(\text{data}|\Delta h_0, H)$ is computed by using both the statistical distribution ρ_s of the synthetic spectra and the probability density $\rho_d(f, E)$ of the experimental spectrum (i.e. the data). In practice, the conditional probability is computed through (Tarantola & Valette 1982)

$$\rho(\text{data}|\Delta h_0, H) = \int\int \rho_s(f, E|\Delta h_0, H)\rho_d(f, E)df dE, \quad (8)$$

where the dependence of ρ_s with respect to the parameters Δh_0 and H has been made explicit.

Depending on the experimental situation the probability ρ_d can be a more or less complicated expression. For instance, the statistical distribution of several experimental spectra corresponding to independent averaging profiles could be used to obtain ρ_d. In the present study, no such statistical analysis can be done since a single averaging y profile is available. Consequently,

$$\rho_d(f, E) = \delta\big(f, E - |\langle\psi_f\rangle_L|^2\big), \quad (9)$$

where δ is the 2-D Dirac distribution, and eq. (8) reduces to a curvilinear integral along the experimental spectral curve. In practice, for the examples shown in Fig. 5, the probability $\rho(\text{data}|\Delta h_0, H)$ in eq. (8) equals the integral of the probability $\rho_s(f, E|\Delta h_0, H)$ along the thick black lines representing the experimental spectrum.

The prior probability density $\rho(\Delta h_0, H)$ in eq. (7) may take very different forms depending on the prior information available. In the present study, we simply use a uniform distribution in the $(\Delta h_0, H)$ domain.

The solution of the inverse problem is obtained by computing the posterior probability density $\rho_p(\Delta h_0, H|\text{data})$ given by eq. (7) with the probability distributions in eqs (8) and (9). Both the numerical lightness of the stochastic forward problem and the low (2) dimension of the parameter space allow the posterior probability to be mapped by performing a systematic scan of a limited domain of the parameter space.

A contour map of ρ_p is shown in Fig. 6 for a wide $(\Delta h_0, H)$ domain. It can be seen that the posterior probability map possesses a single high-probability domain with a limited size. The high-probability domain is elongated in the Δh_0 axis direction and narrower along the H axis. The small negative slope of the major axis of the high-probability domain indicates a slight correlation between the two inverted parameters: the larger the Hurst exponent H the smaller the range Δh_0. The model with the maximum posterior probability (black star in Fig. 6) is for $\Delta h_0 = 12$ mm and $H = 0.74$.

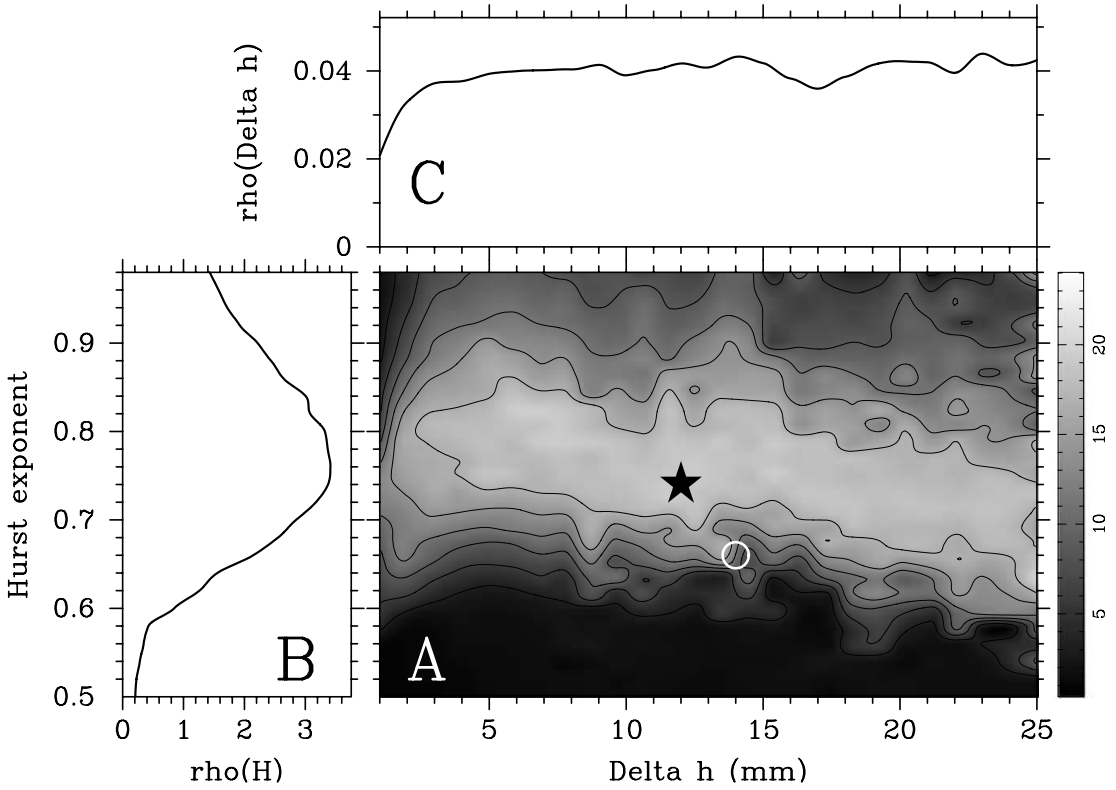

Figure 6. (a) Posterior probability density resulting from the inversion of the spectrum of the mean backscattered waves shown in Fig. 5. The black star corresponds to the model with the highest posterior probability ($\Delta h_0 = 12$ mm, $H = 0.74$), and the white circle is for $\Delta h_0 = 14$ mm and $H = 0.66$ (see also Fig. 5). (b) Marginal posterior probability for the parameter H obtained by integrating the 2-D posterior probability density shown in (a) (see eq. 10). (c) Marginal posterior probability for the parameter Δh_0.

The Hurst exponent H is a well-resolved parameter as can be observed in the marginal-probability curve

$$\rho_{\mathrm{p}}(H) \equiv \int \rho_{\mathrm{p}}(\Delta h_0, H)\, d\Delta h_0, \tag{10}$$

which shows (Fig. 6b) that the most probable values for H are in the range 0.72–0.80. This agrees with the experimental determination of H equal to 0.72 ± 0.08 (Gautier & Gibert 2004).

The marginal probability curve

$$\rho_{\mathrm{p}}(\Delta h_0) \equiv \int \rho_{\mathrm{p}}(\Delta h_0, H)\, dH \tag{11}$$

shown in Fig. 6(c) does not display a clear maximum and confirms that the amplitude range Δh_0 is a poorly resolved parameter despite the fact that the experimental values for Δh_0 fall in a rather narrow Gaussian range as shown in Fig. 7. This agrees with the preliminary sensitivity tests, in which variations of Δh_0 do not produce significant changes in the slope of the synthetic spectra which constitutes the main information used in the inversion. We found that the amplitude ψ_0 (eq. 6) is the observable quantity that is the most affected by changes in the amplitude range Δh_0. Unfortunately, as stated above, ψ_0 is rarely measured in real field conditions because of absolute calibration problems, and this is why we do not use this information in the inversion.

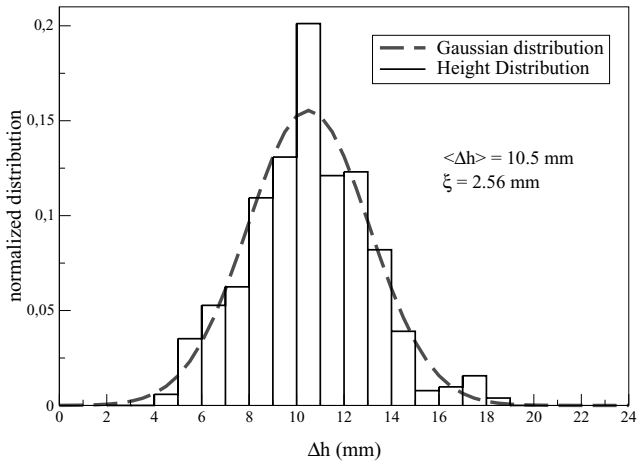

Figure 7. Histogram of the Δh_0 values experimentally determined from a set of topography profiles (e.g. Fig. 1) measured on the resin print used in the experiments. The histogram is reasonably fitted ($\chi^2 = 2 \times 10^{-4}$) with a Gaussian distribution (dashed curve) with a mean $\langle \delta h_0 \rangle = 10.5$ mm and a standard deviation $\xi = 2.56$ mm.

5 CONCLUSION

The determination of the roughness parameters, the Hurst exponent H and the amplitude range Δh_0, of fractal surfaces from backscattered waves is difficult because of the long-range correlation of the self-affine topography. The energy spectra of the backscattered waves averaged along profiles of finite length display strong fluctuations corresponding to the mesoscopic scales of the particular averaging profiles chosen. In order to account for these mesoscopic phenomena, it is necessary to consider the backscattering forward problem as a stochastic process whose output differs at each run in order to restitute the random variability observed in the data. This

approach is used in a single-scattering modelling assuming a near-nadir and far-field geometry. A Bayesian inversion is used to account for the stochastic nature of both the data and the forward problem. A map of the posterior probability $\rho_p(\Delta h_0, H|\text{data})$ is drawn by scanning a region of the $(\Delta h_0, H)$ domain. This map constitutes the general solution of the inverse problem from which the most probable models can easily be inferred. The inversion of a spectrum obtained along a single averaging profile shows that the Hurst exponent H is a well-resolved parameter, as can be inferred from the marginal probability curve. On the other hand, the amplitude range Δh_0 is a very poorly resolved parameter for which it is only possible to obtain an order-of-magnitude estimate. Sensitivity tests show that a more accurate determination of Δh_0 could probably be obtained if an absolute calibration of the source amplitude ψ_0 were available.

ACKNOWLEDGMENTS

We thank Frédéric Conil for his assistance during the experiments and Arnaud Derode for fruitful scientific discussions. Marc Pessel and an anonymous reviewer made very constructive comments. This study was financially supported by the CNRS and ANDRA through the GdR FORPRO (Research action number 99.II) and corresponds to GdR FORPRO contribution number 2003/13 A.

REFERENCES

Angelsen, B.A., 2000. *Ultrasound Imaging: Waves, Signals, and Signal Processing,* Emantec, Norway.

Beckmann, P. & Spizzichino, A., 1963. *The Scattering of Electromagnetic Waves from Rough Surfaces,* Artech House Publishers.

Berry, M.V., 1972. On deducing the form of surfaces from their diffracted echoes, *J. Phys. A,* **5**, 272–291.

Berry, M.V., 1979. Diffractals, *J. Phys. A,* **12**, 781–797.

Berry, M.V. & Blackwell, T.M., 1981. Diffractal echoes, *J. Phys. A,* **14**, 3101–3110.

Brown, S.R., 1989. Transport of fluid and electric current through a single fracture, *J. geophys. Res.,* **94**, 9429–9438.

Burrough, P.A., 1981. Fractal dimensions of landscapes and other environmental data, *Nature,* **294**, 240–242.

Campbell, B.A. & Shepard, M.K., 1996. Lava flow surface roughness and depolarized radar scattering, *J. geophys. Res.,* **101**, 18 941–18 951.

Chen, J., Titus, K.Y., Lo Leung, H. & Litva, J., 1994. The use of fractals for modeling EM waves scattering from rough sea surface, *IEEE Trans. Geosci. Remote Sens.,* **34**, 966–972.

Conil, F., Gibert, D. & Nicollin, F., 2004. Non-linear synthesis of input signals in ultrasonic experimental setups, *J. acoust. Soc. Am.,* **115**, 246–252.

Elmore, W.C. & Heald, M.A., 1985. *Physics of Waves,* Dover, New York.

Feder, J., 1988. *Fractals,* Plenum, New York.

Fox, C.G., 1987. An inverse Fourier transform algorithm for generating random signals of a specified spectral form, *Comput. Geosci.,* **13**, 369–374.

Fox, C.G. & Hayes, D.E., 1985. Quantitative methods for analyzing the roughness of the seafloor, *Rev. Geophys.,* **23**, 1–48.

Gautier, S. & Gibert, D., 2004. Scattering from a fractal surface: Acoustical experiments and comparison with near-nadir models, *Icarus,* **167**, 453–463.

Gibert, D. & Virieux, J., 1991. Electromagnetic imaging and simulated annealing, *J. geophys. Res.,* **96**, 8057–8067.

Goff, J.A. & Jordan, T.H., 1989. Stochastic modeling of seafloor morphology: Inversion of sea beam data for second-order statistics, *J. geophys. Res.,* **93**, 13 589–13 609.

Gouyet, J.F., 1992. *Physique et Structures Fractales,* Masson, Paris.

Ishimaru, A., 1997. *Propagation and Scattering in Random Media: Multiple Scattering, Turbulence, Rough Surfaces, and Remore Sensing,* Oxford Univ. Press, Oxford.

Jackson, D.R., Briggs, K.B., Williams, K.L. & Richardson, N.D., 1996. Tests of models for high-frequency seafloor backscattering, *IEEE J. Ocean. Engin.,* **21**, 458–470.

Jaggar, D.L. & Sun, X., 1990. Scattering from fractally corrugated surfaces, *J. opt. Soc. Am.,* **7**, 6.

Lurton, X., 2002. *An Introduction to Underwater Acoustics,* Springer Verlag, Berlin–New York.

Lyons, A.P., Anderson, A.L. & Dwan, F.S., 1994. Acoustic scattering from seafloor: Modeling and data comparison, *J. acoust. Soc. Am.,* **95**, 2441–2451.

Mandelbrot, B.B., 1975. Stochastic models for the Earth's relief, the shape and the fractal dimension of coastlines, and the number-area rule for islands, *Proc. Nat. Acad. Sci. USA,* **72**, 3825–3828.

Meheust, Y. & Schmittbuhl, J., 2000. Flow enhancement of a rough fracture, *Geophys. Res. Lett.,* **27**, 2989–2992.

Milne, B.T., 1988. Measuring the fractal geometry of landscapes, *Appl. Math. Comput.,* **27**, 67–79.

Mourad, P.D. & Jackson, D.R., 1993. A model/data comparison for low-frequency bottom backscatter, *J. acoust. Soc. Am.,* **94**, 344–358.

Ogilvy, J.A., 1991. *Theory of Wave Scattering from Random Rough Surfaces,* IOP, Bristol.

Okubo, P.G. & Aki, K., 1987. Fractal geometry in the San Andreas Fault system, *J. geophys. Res.,* **92**, 345–355.

Papoulis, A., 1984. *Probability, Random Variables and Stochastic Processes,* McGraw-Hill, New York.

Press, W.H., Teukolsky, S.A., Vetterling, W.K. & Flannery, B.P., 1992. *Numerical Recipes in FORTRAN 77,* Cambridge Univ. Press, New York.

Sayles, R.S. & Thomas, T.R., 1978. Surface topography as a non-stationary random process, *Nature,* **271**, 431–434.

Schmittbuhl, J., Gentier, S. & Roux, S., 1993. Field measurements of roughness of fault surfaces, *Geophys. Res. Lett.,* **20**, 639–641.

Shepard, M.K. & Campbell, B.A., 1999. Radar scattering from a self-affine fractal surface: Near-nadir regime, *Icarus,* **141**, 156–171.

Shepard, M.K., Campbell, B.A., Bulmer, M., Farr, T., Gaddis, L.R. & Plaut, J., 2001. The roughness of natural terrain: A planetary and remote sensing perspective, *J. geophys. Res.,* **106**, 32 777–32 795.

Simonsen, I., Vandembroucq, D. & Roux, S., 2000. Wave scattering from self-affine surfaces, *Phys. Rev. E,* **61**, 5914–5917.

Smith, D.K. & Shaw, P.R., 1989. Using topographic slope distributions to infer seafloor patterns, *IEEE J. ocean. Eng.,* **14**, 338–347.

Tarantola, A. & Valette, B., 1982. Inverse problems = Quest for information, *J. Geophys.,* **50**, 159–170.

Thompson, M.E. & Brown, S.R., 1991. The effect of anisotropy surface roughness on flow and transport in fractures, *J. geophys. Res.,* **96**, 21 923–21 932.

Turcotte, D.L., 1989. Fractals in geology and geophysics, *Pure appl. Geophys.,* **131**, 171–196.

Voronovich, A.G., 1994. *Wave Scattering from Rough Surfaces,* Springer Verlag, Berlin–New York.

Zribi, M., Ciarletti, V. & Taconet, O., 2000. Validation of a rough surface model based on fractional Brownian geometry with SIRC and ERASME radar data over Orgeval, *Remote Sens. Environ.,* **73**, 65–72.